The Role of Phosphorus Dioxide in the H + OH Recombination Reaction: Ab Initio Quantum Chemical Computation of Thermochemical and Rate Parameters

Naomi L. Haworth, George B. Bacskay,* and John C. Mackie

School of Chemistry, University of Sydney, NSW 2006, Australia

Received: July 11, 2001; In Final Form: November 7, 2001

A theoretical investigation of the effects of PO_2 on the H + OH radical recombination reaction is reported. The focus of the study is the computation of rate coefficients by ab initio quantum chemical and RRKM methods for the H + PO_2 and OH + PO_2 recombination reactions and for the H + HOPO → H_2 + PO_2, OH + H_2 → H + H_2O, and H + $HOPO_2$ → H_2O + PO_2 abstraction reactions, which constitute a catalytic pathway for the H + OH recombination reaction (Twarowski, A. *Combust. Flame* **1993**, *94*, 91). These are a subset of Twarowski's reaction model (Twarowski, A. *Combust. Flame* **1995**, *102*, 41) that consists of 175 individual reactions and includes 17 phosphorus-containing molecules. The thermochemistry of this complete reaction model was computed using the Gaussian methods: G2, G3, and G3X. While G3X was found to be superior to G2 and G3 for the prediction of heats of formation of phosphorus-containing molecules, it underestimates the heat of formation of $HOPO_2$ by at least 3.6 kcal mol^{-1}, when compared with the extensive coupled cluster computations of Bauschlicher (Bauschlicher, C. W., Jr. *J. Phys. Chem.* **1999**, *103*, 11126). Consequently, the rate coefficients reported in this work are based on Bauschlicher's thermochemical data for PO_2, HOPO, and $HOPO_2$. The computed rate coefficients are consistent with the available experimental data and the results of modeling studies by Twarowski (Twarowski, A. *Combust. Flame* **1995**, *102*, 41) and Korobeinichev et al. (Korobeinichev, O. P.; Ilyin, S. B.; Bolshova, T. A.; Shvartsberg, V. M.; Chernov, A. A. *Combust. Flame* **2001**, *125*, 744). The recombination reactions are found to be substantially into the fall-off region at near atmospheric pressures.

Introduction

The recombination reaction of H and OH radicals to form water is a key exothermic reaction in a range of combustion processes, particularly in flames and in the combustion of hydrogen fuel in the presence of oxygen. As pointed out by Twarowski,[1−4] this last reaction is of special importance in supersonic aircraft engines, where recombination must be as fast as possible in order to maximize engine efficiency. Twarowski carried out a number of experimental studies of the H + OH recombination reaction in the presence of phosphine and concluded the reaction is catalyzed by oxidation products of PH_3, namely PO_2, HOPO, and $HOPO_2$. Two possible reaction sequences were proposed to account for this catalysis:

$$H + PO_2 (+ M) \rightarrow HOPO (+ M) \quad (1a)$$

$$H + HOPO \rightarrow H_2 + PO_2 \quad (1b)$$

$$OH + H_2 \rightarrow H_2O + H \quad (1c)$$

and

$$OH + PO_2 (+ M) \rightarrow HOPO_2 (+ M) \quad (2a)$$

$$H + HOPO_2 \rightarrow H_2O + PO_2 \quad (2b)$$

The net result of both sets of reactions is the recombination reaction of interest:

$$H + OH \rightarrow H_2O \quad (3)$$

The full reaction model put forward by Twarowski[3] consists of 175 reactions involving 24 species, 17 of which contain P atoms. A serious limitation of the model has been the lack of reliable rate and thermochemical data; the rate coefficients of 162 of these reactions were estimated by Benson's rules.[5]

This work aims to remedy the situation by computing the heats of formation of the phosphorus-containing molecular species in Twarowski's model[3] and rate coefficients for the critical reactions that make up the catalytic cycles (eqs 1) and (eqs 2) given above, using Gaussian-2 (G2),[6] Gaussian-3 (G3),[7] and Gaussian-3X (G3X)[8] as well as other ab initio quantum chemical methods. The applicability and reliability of the Gaussian methods to phosphorus-containing molecules such as PO_2, HOPO, and $HOPO_2$ are tested by comparing the results obtained with those from other studies using alternative methods such as the coupled cluster method. Given the documented catalytic properties of these simple phosphorus-containing molecules it is highly likely that these, as well as various organic derivatives, would be efficient fire retardants. The work reported here was motivated to a large extent by this idea and represents the initial steps of a study that focuses on the investigation of the flame suppression mechanisms by organophosphorus compounds, using both computational and experimental techniques. Achieving an improved level of understanding of the mechanisms of flame suppression by these species has the potential to provide guidance for the development of efficient and environmentally friendly fire retardants. Indeed, it has been shown recently that dimethyl methylphosphonate (DMMP) or trimethyl phosphate (TMP) when added to flames retard the

* Corresponding Author. E-mail: bacskay@chem.usyd.edu.au.

10.1021/jp012649b CCC: $22.00
Published on Web 02/02/2002

flame velocity with an efficiency comparable with that of CF_3Br.[9] This agent, prior to the Montreal protocol, was in widespread use as a fire suppressant, especially for aircraft engines and in military applications. A further potential bonus of phosphorus compounds is that they can be added to polymer blends whereby they can act as condensed phase inhibitors promoting the formation of chars to inhibit the burning of plastics; upon vaporization they also act as vapor-phase inhibitors.[10]

A further recent interest in phosphorus flame chemistry has arisen from the need to destroy toxic chemical waste and chemical warfare agents such as sarin.[11] Recent investigations[12,13] of incineration of these agents have involved a study of the combustion of organophosphorus compounds, including DMMP and TMP as models for sarin. Korobeinichev et al.[12] measured the concentrations of PO, PO_2, HOPO, and $HOPO_2$ in the burnt gases of premixed low-pressure flames of H_2/O_2/Ar doped with DMMP. Using kinetic modeling, they optimized rate coefficients for key phosphorus flame gas reactions to their measured profiles. They concluded that organophosphorus additives can actually promote low-pressure H_2/O_2/Ar flames. In a subsequent study[13] they found, however, that TMP inhibits atmospheric CH_4/O_2/Ar and H_2/O_2/Ar flames. Macdonald et al.[14] found that the inhibiting ability of DMMP in nonpremixed CH_4/O_2/Ar flames diminishes with increasing adiabatic flame temperature. The ability to model these inhibition and promotion characteristics of organophosphorus additives to flames is very dependent on the availability of reliable rate coefficients for key phosphorus flame reactions over a wide range of pressures and temperatures.

Theory and Computational Methods

The heats of formations of approximately 30 molecules were obtained by quantum chemical computations of energies and enthalpies, utilizing the Gaussian methods (G2, G3, and G3X) of Pople and co-workers.[6−8] In these approaches the energies of the atomic and molecular species of interest are obtained via quadratic configuration interaction (QCISD(T)) calculations in small valence triple and double-ζ + polarization functions bases (6-311G(d,p) and 6-31G(d)), respectively, which are then corrected by MP4, MP2, and SCF estimates of the energy changes with systematic enlargement of the basis sets and by empirical higher level corrections. Open shell systems are treated by the unrestricted versions of the above approaches. The heats of formation at 298 K are obtained from the computed G2, G3, and G3X values of the atomization energies (at 0 K) in conjunction with experimental heats of formation of the elements in their atomic states and thermal corrections, as discussed in detail by Curtiss et al.[15] For some radical species (particularly PO), a variant of the G3(RAD) approach of Radom and coworkers,[16−18] was also used, where the unrestricted Hartree−Fock (UHF) and Møller−Plesset (UMP) computations are replaced by their restricted open shell ROHF and ROMP analogues, while the (unrestricted) quadratic CI (QCISD(T)) method[19] implicit in G2 and G3 is replaced by the restricted singles and doubles coupled cluster method with perturbative correction for triples (RCCSD(T)).[20,21]

The rates of the reactions in Twarowski's reaction sequence were determined using transition state theory (TST).[22] In the case of reactions with well-defined transition states, viz. first-order saddle points, the G3 method was used, whereby the saddle points were located at the appropriate SCF and MP2 levels of theory. Using the appropriate energies and partition functions, the limiting high-pressure rate coefficient k_∞ at any given temperature T is then obtained from the equation

$$k_\infty(T) = \frac{k_B T}{h} \frac{q^\ddagger}{q_A q_B \ldots} \exp\left(-\frac{E_c}{k_B T}\right) \quad (4)$$

where E_c is the critical energy of reaction, k_B is the Boltzmann constant, h is Planck's constant, $q^\ddagger$ is the partition function of the transition state, and q_A, q_B,... are the partition functions of the reactants A, B,.... The latter are obtained readily from the computed rotational constants and vibrational frequencies, using the standard formulas of statistical mechanics, with the rigid rotor and harmonic vibrations approximations.[23] The computed rate coefficients, over a range of temperatures, could then be fitted to the standard Arrhenius form

$$k_\infty(T) = A \exp\left(-\frac{E_a}{k_B T}\right) \quad (5)$$

where E_a is the activation energy and A is the Arrhenius preexponential factor. Rate coefficients were generated at 1000, 1250, 1500, 1750, and 2000 K. These temperatures gave a sensible range over which rate coefficients could be fitted and spans the temperatures studied by Twarowski[1−4] and Korobeinichev.[13] Alternatively, the rate coefficients could be fitted to a modified Arrhenius equation, viz.

$$k_\infty(T) = AT^n \exp\left(-\frac{E_a}{k_B T}\right) \quad (6)$$

As a number of the reactions studied are barrierless recombinations, with no saddle-point to define the transition state, variational transition state theory (VTST)[24a−c] was used to calculate the appropriate rate coefficients. These calculations were carried out by evaluating the rate coefficients k_{dis} of the (reverse) dissociation reactions along the intrinsic reaction coordinate and thus locating the geometry (at a given temperature) where the rate coefficient is a minimum.[25,26] As such transition states generally correspond to molecules near a bond dissociation limit, the VTST geometries were located via complete active space SCF (CASSCF) calculations,[27,28] using Dunning's correlation consistent cc-pVDZ basis sets.[29,30] The active spaces in these CASSCF calculations (on H + PO_2 and OH + PO_2 transition states) typically correspond to 8−18 active electrons in 6−13 active orbitals. The critical energy of the dissociation reaction is then obtained by correcting the dissociation energy obtained by G3 or other high level theory, by the computed energy difference between the dissociated system and the transition state that had been determined at the CASSCF/cc-pVDZ level of theory. In the case of reaction 2a the energy difference was recalculated using complete active space second-order perturbation (CASPT2)[31,32] theory in conjunction with Dunning's cc-pVTZ basis. (Use of a higher level of theory and larger basis set, as exemplified by the CASPT2/cc-pVTZ approach, is expected to yield more reliable energies than the lower level CASSCF/cc-pVDZ method that was employed for the determination of geometries and frequencies.) The rate coefficient k_{ass} for the association reaction is then obtained from the equation

$$\frac{k_{ass}}{k_{dis}} = K_c \quad (7)$$

where K_c is the equilibrium constant for the association

(recombination) reaction and which is readily calculated at any temperature from the appropriate Gibbs free energy of reaction, $\Delta_r G$.

The pressure dependence of the dissociation rate coefficients in a bath gas of N_2 was determined via the RRKM model in the weak collision approximation, using an average collisional energy transfer parameter of 400 cm^{-1}, at pressures ranging from 1 to 10^4 Torr and temperatures 1000−2000 K. To have the rate coefficients in a convenient form for use by combustion modelers the RRKM rate coefficients were then expressed in terms of a Troe fit,[33] as defined by the equations

$$\frac{k}{k_\infty} = \left(\frac{k_0/k_\infty}{1 + k_0/k_\infty}\right) F(k_0/k_\infty) \tag{8}$$

$$\log F(k_0/k_\infty) = \frac{\log F_{cent}}{1 + \left[\dfrac{\log (k_0/k_\infty) + c}{N - \mathrm{d}(\log (k_0/k_\infty) + c)}\right]^2} \tag{9}$$

where

$$c = -0.4 - 0.67 \log(F_{cent}) \tag{10}$$

$$N = 0.75 - 1.27 \log(F_{cent}) \tag{11}$$

$$d = 0.14 \tag{12}$$

and

$$F_{cent} = (1 - a) \exp\left(-\frac{T}{T^{***}}\right) + a \exp\left(-\frac{T}{T^{*}}\right) + \exp\left(-\frac{T^{**}}{T}\right) \tag{13}$$

k_0 is the pseudo-first-order limiting low-pressure rate coefficient, i.e., equal to the bimolecular rate coefficient multiplied by the bath gas concentration. k_∞ is the high-pressure rate coefficient calculated by transition state theory. a, T^*, T^{**}, and T^{***} are fitted parameters expressing the variation with temperature of the pressure-dependent rate coefficients.

All G2, G3, and G3X calculations were carried out using the Gaussian98 programs.[34] The ROMP and RCCSD(T) computations were performed using ACESII,[35] while DALTON[36] and MOLCAS4[37] were used for the CASSCF geometry optimizations and CASPT2 energy calculations, respectively. The CHEMRATE[38] programs were employed for the RRKM calculations. All computations were performed on DEC alpha 600/5/333 and COMPAQ XP1000/500 workstations of the Theoretical Chemistry group at the University of Sydney.

Results and Discussion

G2, G3, and G3X Thermochemistry. The energies and heats of formation of the 24 species involved in Twarowski's reaction schemes,[1−4] calculated using the G2, G3, and G3X methods, are given in Table 1. As will be discussed later, the standard G3 and G3X results for PO (based on spin unrestricted calculations) are regarded as unreliable. We recommend instead the G3(RAD) and G3X(RAD) values, which are also listed in Table 1. Where available, experimental and/or other theoretical heats of formation[39−43] are also listed for comparison. The computed equilibrium geometries, rotational constants, and vibrational frequencies are listed in Table S1 of the Supporting Information. A number of species, such as P_2O_2, have several geometric isomers as well as low lying excited electronic states, giving rise to potential uncertainties as to the nature of the ground electronic state. In such cases all possible isomers as well as a range of electronic states were explicitly considered in the calculations. The results in Tables 1 and S1 pertain to the electronic ground states thus located, for the lowest energy isomers.

Comparison with the available experimental data suggests that for most systems the difference between theory and experiment is ∼2 kcal mol^{-1} or less. For some molecules, however, notably P_4 and $HOPO_2$, the difference between the G3 result and experiment can be up to ∼4 kcal mol^{-1}. The G3X results, as expected, are generally superior to those obtained by G3. However, quite large discrepancies are noted when we compare the G3 and G3X heats of formations with those calculated by Bauschlicher.[42] The latter were obtained by extrapolation of (R)CCSD(T) energies, obtained with the cc-pVXZ (for P and H) and aug-cc-pVXZ (for O) basis sets (X = T, Q, 5), to the complete basis set (CBS) limit, and include core−valence correlation corrections, scalar relativistic, and spin−orbit corrections. Given the discrepancies between the G3X and Bauschlicher's CBS heats of formation, in our computation of rate coefficients and reaction enthalpies we use Bauschlicher's recommended values for PO_2, HOPO, and $HOPO_2$. The demonstrated weakness of the Gaussian approach for some of these systems is further analyzed in the next section.

HOPO and $HOPO_2$, which are particularly important species in Twarowski's reaction scheme,[1−4] possess low-frequency torsional modes. Treating these as harmonic oscillators in the calculation of partition functions might be expected to affect the accuracy of the computed thermal contributions. We checked the reliability of the harmonic model in these cases by computing full (360°) torsional potentials by a series of MP2/6-31G(d) calculations (at 5−10 degree intervals) and the corresponding energy eigenvalue spectra and partition functions. For HOPO the torsional partition function was found to be 5.05 at 2000 K, viz., the highest temperature of interest, indicating that effectively only the fifth torsional energy level was available to the molecule. The energy of this level was 6.08 kcal mol^{-1} above the minimum in the potential, which corresponds to being 4.42 kcal mol^{-1} below the height of the barrier to rotation. Consequently, no rotation would be expected to occur in this molecule. Similarly, for $HOPO_2$ the torsional partition function at 2000 K was computed to be 7.74, indicating occupancy of the seventh torsional level, which has an energy of 4.45 kcal mol^{-1}, and which again is significantly lower than the rotational barrier of 7.68 kcal mol^{-1}. The hindered rotor correction therefore would result in insignificant changes in the molecular partition functions. Thus, use of the all-vibration model for the computation of thermal corrections has been validated.

The reaction enthalpies for the 175 reactions that make up Twarowski's scheme,[1−4] as obtained from our calculated heats of formation, are listed in Table S2 of the Supporting Information.

Reliability of G3, G3X, and Related Methods. As noted above, our G3 heats of formation for a number of phosphorus-containing molecules, especially P_4, PO_2, PO_3, and $HOPO_2$, differ by up to ∼6 kcal mol^{-1} from experiment or the computed values of Bauschlicher.[42] Errors of this magnitude were found for several other non-hydrogen systems such as SF_6 and PF_5,[44] although these problems appear to have been overcome by the recent introduction of G3X.[8] Consequently, testing G3X on some of the problem molecules encountered in this work is particularly relevant.

G3X differs from G3 in three major respects: the calculation of geometries and vibrational frequencies (at B3LYP/6-31G(2df,1p) level in G3X) and a SCF energy correction for basis

TABLE 1: Total Energies and Heats of Formation Computed at G2, G3, and G3X Levels of Theory

species	E_o(0 K)/E_h			$\Delta_f H_{298}{}^0$/kcal mol^{-1}			
	G2	G3	G3X	G2	G3	G3X	literature[a]
H	−0.50000	−0.49959	−0.50097				52.1030 ± 0.0014[b]
O	−74.98203	−75.02957	−75.03224				59.553 ± 0.024[b]
P	−340.81821	−341.11502	−341.11699				75.62 ± 0.24[b]
H_2 − $^1\Sigma_g$ ($D_{\infty h}$)	−1.16636	−1.16738	−1.16721	−1.1	−0.5	−0.4	0.0
O_2 − $^3\Sigma_g$ ($D_{\infty h}$)	−150.14821	−150.24821	−150.25248	2.4	1.1	0.0	0.0
P_2 − $^1\Sigma_g$ ($D_{\infty h}$)	−681.81931	−682.41600	−682.41907	35.6	35.5	34.3	34.3 ± 0.5[b]
P_4 − $^1A_1$ (T_d)	−1363.71963	−1364.91465	−1364.92008	19.6	18.2	16.2	14.1 ±0.05[b]
OH − $^2\Pi$ ($C_{\infty v}$)	−75.64391	−75.69490	−75.69607	9.1	8.4	8.4	9.32 ± 0.29[b]
							8.83 ± 0.09[c]
H_2O − $^1A_1$ (C_{2v})	−76.33205	−76.38204	−76.38323	−58.1	−57.5	−57.5	−57.798 ± 0.010[b]
HO_2 − $^2A''$ (C_s)	−150.72792	−150.82689	−150.82950	3.3	3.3	3.2	0.5 ± 2.0[b]
PH − $^3\Sigma$ ($C_{\infty v}$)	−341.42844	−341.73033	−341.73131	57.7	56.0	55.7	*60.6 ± 8.0*[d]
PH_2 − $^2B_1$ (C_{2v})	−342.04913	−342.34974	−342.35096	32.9	32.6	32.2	*26 ± 23*[e]
PH_3 − $^1A'$ (C_s)	−342.67900	−342.97851	−342.98004	2.0	3.1	2.4	1.3 ± 0.4[b]
PO − $^2\Pi$ ($C_{\infty v}$)	−416.02430	−416.37332	−416.38022	−6.4	−7.6	−10.8	−5.6 ± 1.0[b]
					−7.1[f]	−7.7[f]	−6.8 ± 1.9,[g] *−7.8*[h]
PO_2 − $^2A_1$ (C_{2v})	−491.19500	−491.59301	−491.59877	−66.4	−67.5	−69.2	−66.6 ± 2.6[g]
					−69.1[f]	−70.2[f]	*−70.3*[h]
PO_3 − $^2A_2'$ (D_{3h})	−566.32361	−566.77130	−566.78381	−100.1	−101.7	−106.3	*−107.5*[h]
PO_3 − $^2B_2$ (C_{2v})		−566.77102			−101.4		
PPO − $^1\Sigma$ ($C_{\infty v}$)	−756.94248	−757.58837	−757.59417	5.8	5.5	3.3	
P_2O − $^1A_1$ (C_{2v})	−756.93141	−757.57613		12.7	13.1		
P_2O_2 − planar − ^1A_g (D_{2h})	−832.12205	−832.81642	−832.82515	−59.8	−59.8	−63.4	
P_2O_2 − butterfly (C_1)	−832.10890	−832.80295		−51.8	−51.6		
P_2O_2 − cis − $^3A''$ (C_s)	−832.10775	−832.80583		−50.7	−53.0		
P_2O_2 − trans − $^3A''$ (C_s)	−832.10457	−832.80259		−48.5	−50.8		
P_2O_3 − gauche − ^1A (C_2)	−907.34228	−908.08682	−908.09849	−150.3	−151.1	−155.3	
HPO − $^1A'$ (C_s)	−416.62879	−416.97614	−416.98030	−21.1	−20.5	−22.0	*−22.6*[h]
POH − $^3A''$ (C_s)	−416.59568	−416.95018		−0.2	−4.2		
HPOH − trans − $^2A''$ (C_s)	−417.21175	−417.56145	−417.56447	−22.2	−22.5	−23.4	
HPOH − cis − $^2A''$ (C_s)	−417.21070	−417.56045		−21.4	−21.7		
H_3PO − $^1A_1$ (C_{3v})	−417.83301	−418.18166	−418.18604	−47.9	−46.9	−48.6	
H_2POH − trans − $^1A'$ (C_s)	−417.83334	−418.18206	−418.18558	−47.8	−46.8	−48.0	
H_2POH − cis − $^1A'$ (C_s)	−417.83292	−418.18168		−47.6	−46.7		
HOPO − cis − $^1A'$ (C_s)	−491.84249	−492.23992	−492.24608	−108.1	−108.3	−110.3	−110.6 ± 3[i]
							−112.4[h]
HOPO − trans − $^1A'$ (C_s)	−491.83848	−492.23577		−105.6	−105.7		
HPO_2 − $^1A_1$ − C_{2v}	−491.82318	−492.22032		−96.1	−96.1		
$HOPO_2$ − planar − $^1A'$ (C_s)	−567.00756	−567.45385	−567.46232	−164.7	−164.8	−167.4	−168.8 ± 4[i]
							−171.4[h]

[a] Experimental values unless otherwise indicated by italics and footnotes. [b] Ref 39. [c] Ref 40. [d] Semiempirical estimate, ref 39. [e] Estimate, ref 39. [f] Computed by G3(RAD) and G3X(RAD) type procedures. [g] Ref 41. [h] RCCSD(T)/CBS computations, ref 42. [i] Ref 43.

TABLE 2: Phosphorus Oxides and Acids: Comparison of Computed Heats of Formation ($\Delta_f H_{298}{}^0$/kcal mol^{-1})[a]

	G3	G3X	G3X2	RCCSD(T)/CBS[b]
PO	−7.3 (−6.8)[c]	−10.5 (−7.4)[c]	−11.9 (−8.8)[c]	−7.8
PO_2	−66.7 (−69.1)[c]	−68.4 (−70.2)[c]	−70.6 (−72.2)[c]	−70.3
PO_3	−100.5	−105.2	−108.3	−107.5
HPO	−19.9	−21.6	−23.6	−22.6
HOPO	−107.5	−109.5	−111.6	−112.4
$HOPO_2$	−163.2	−165.8	−168.8	−171.4

[a] All heats of formation corrected for scalar relativistic effects, as in ref 42. [b] Ref 42. [c] Computed by G3(RAD), G3X(RAD), and G3X2(RAD) type procedures.

set expansion (to G3XLarge in the G3X method). In addition the higher-level correction parameters have been revised.[8] As a small modification to G3X, we propose that we apply the G3XLarge basis set expansion correction at the MP2(full) level, i.e., we simply replace the MP2(full)/G3Large computation with MP2(full)/G3XLarge. This modified G3X technique is denoted G3X2.

Our computed G3X and G3X2 heats of formation are given in Table 2, where they are also compared with the G3 values and Bauschlicher's CBS results.[42] As the latter contain scalar relativistic corrections, we applied the same corrections to the G3, G3X, and G3X2 results, so as to make the comparisons more meaningful. As discussed below, in the case of PO the G3(RAD), G3X(RAD), and G3X2(RAD) results are preferred over their standard (unrestricted) counterparts. With that proviso we may note that going from G3 to G3X and to G3X2 does yield significant improvements. In the case of PO_3 much of the improvement can be traced to the lower zero-point energies at the B3LYP level in comparison with the SCF values, which are used in G3. The (scaled) UB3LYP/6-31G(2df,1p) and UHF/6-31G(d) zero-point energies of PO_3 are 5.65 and 8.20 kcal mol^{-1}, respectively; the 2.6 kcal mol^{-1} difference is thus responsible for 55% of the improvement in the heat of formation of PO_3 that occurs when G3 is replaced by G3X. (In the other systems the differences between the G3X and G3 zero-point energies are less than 0.2 kcal mol^{-1}.) Significant further improvements are obtained, however, with the introduction of the G3X2 method. The heats of formation for PO_2, PO_3, HPO, and HOPO are lowered by a further 2−3 kcal mol^{-1}, so that the G3X2 values are generally within 1 kcal mol^{-1} of Bauschlicher's CBS results.[42] In the case of $HOPO_2$, where Bauschlicher judges the reliability of the CBS heat of formation as ±2 kcal mol^{-1}, the discrepancy between the G3X2 and the CBS values at 2.6 kcal mol^{-1} can still be regarded as acceptable.

The problem with PO, where the improvements in the level of theory appear to destroy the initial agreement between G3

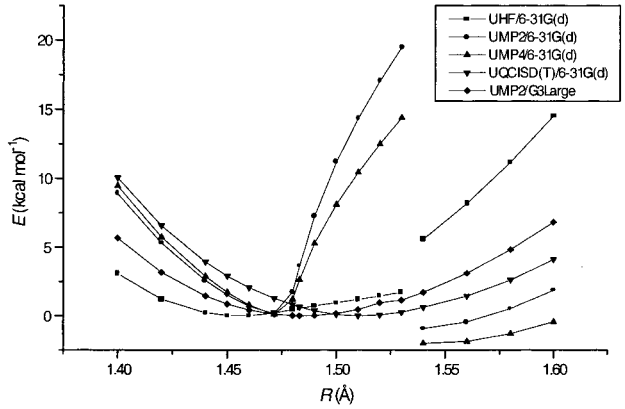

Figure 1. Potential energy curves of PO obtained at unrestricted Hartree−Fock, MP2, MP4, and QCISD(T) levels of theory (relative to respective equilibrium values).

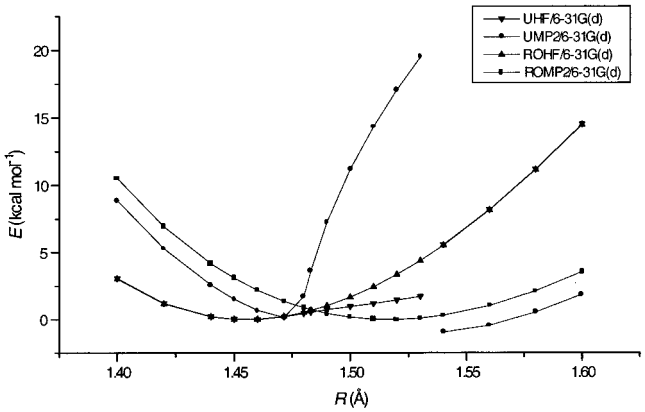

Figure 2. Potential energy curves of PO obtained at restricted and unrestricted Hartree−Fock and MP2 levels of theory (relative to respective equilibrium values).

and CBS, was traced to the presence of spin contamination in the UHF-based calculations that leads to a quite bizarre bond distance dependence. Figure 1 shows the distance dependence of the UHF, UMP2, UMP4, and UQCISD(T) energies, all computed with the 6-31G(d) basis, along with the UMP2/G3L energy. In the region of about 1.47−1.53 Å the UHF energy appears to flatten out, remaining too low, due to a noticeable increase in spin contamination, as indicated by the expectation value of the total spin operator S^2 which increases from 0.76 to 1.16 over the above range of distances. There appears to be a discontinuity at a distance slightly greater than 1.53 Å, so that at 1.54 Å the value of $\langle S^2 \rangle$ has fallen to 0.77 with a corresponding jump in the energy. The UMP2 and UMP4 energies, with a much larger discontinuity, further amplify the un-physical behavior of the UHF wave function and energy. The UQCISD(T) energy shows normal behavior, demonstrating the robustness of the underlying coupled cluster expansion of the wave function to spin contamination in the reference state. Interestingly, when larger, extended basis sets are used, e.g., G3Large, there is only a small blip in the MP2 energy instead of the ∼20 kcal mol^{-1} jump shown by the MP2/6-31G(d) energies. The UHF and UMP2 energies are contrasted with the restricted open shell ROHF and ROMP2 energies in Figure 2. The latter behave in a perfectly sensible manner, with the ROHF energies being near-identical to the UHF energies outside the 1.47−1.53 Å region, but the former smoothly bridge the gap where UHF is discontinuous. In Figure 3 the behavior of the high level theories RCCSD(T), UQCISD(T), and B3LYP are compared. Overall, the UQCISD(T) energies closely match the RCCSD(T) values,

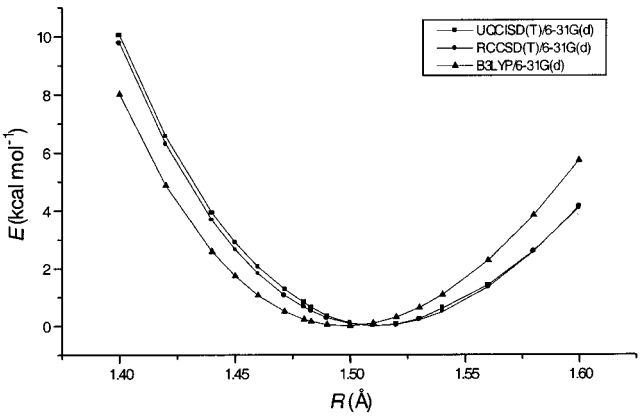

Figure 3. Potential energy curves of PO obtained at unrestricted QCISD(T), B3LYP, and restricted CCSD(T) levels of theory (relative to respective equilibrium values).

although a small blip in the former can now be clearly seen at 1.54 Å. The behavior of the UB3LYP energies is completely sensible and predicts an equilibrium PO distance of ∼1.50 Å, which is ∼0.015 Å lower than the RCCSD(T) value.

In light of the above findings, the unusual behavior of the G3 and G3X results is easy to rationalize. The G3 energies were obtained at the UMP2/6-31G(d) bond distance of 1.4715 Å, i.e., just outside the problem region identified above, and thus a seemingly sensible value for the heat of formation was obtained. The G3X and G3X2 calculations, at the UB3LYP/6-31G(2df,-1p) distance of 1.4988 Å are affected by spin contamination. Note, however, that the UMP2/6-31G(d) value for the bond distance cannot be accepted as reliable, as the corresponding minimum is largely an artifact of the un-physical behavior of the UMP2 energy. In contrast with other (well-behaved) P- and O-containing molecules, where the MP2 PO distances are typically ∼0.02 Å *longer* than the B3LYP values, in PO the UMP2 distance is actually ∼0.03 Å shorter than the UB3LYP value. Therefore, the seemingly sensible heat of formation of PO at the G3 level is fortuitous.

As a further test of the G3, G3X, and G3X2 methods, the atomization energies of PO, PO_2, PO_3, HPO, HOPO, and $HOPO_2$, obtained at the above levels of theory are summarized in Table 3, along with the atomization energies computed at the QCISD(T,full) level of theory using both the G3Large and G3XLarge basis sets, with the higher level correction terms implicit in the G3 techniques included. Such a comparison of G3 and QCI results is relevant since the Gaussian methods aim to produce reliable estimates of the QCISD(T,full) energies in the largest basis sets used, viz., G3Large and G3XLarge, by applying a series of lower level quantum chemical methods in conjunction with a range of basis sets. In the case of the PO and PO_2 radicals the standard UHF-based results are compared with those obtained by the appropriate ROHF-based techniques. The latter are analogous to Radom's G3(RAD) and related methods.[16−18] Finally, comparisons are also made with Bauschlicher's (R)CCSD(T) results.[42] In all cases G3 reproduces the QCISD(T,full)/G3Large atomization energies to within ∼1 kcal mol^{-1}, but mostly better. Similarly, G3X2 reproduces the QCISD(T,full)/G3XLarge atomization energies to within ∼1.5 kcal mol^{-1}, except in the case of PO, where the discrepancy is ∼2.3 kcal mol^{-1}, for the UHF-based calculations. The consistency of the ROHF-based results is significantly better. Comparison with Bauschlicher's results demonstrates that the G3X2 method is capable of yielding chemically accurate atomization energies and hence heats of formation for this class of difficult molecules. The worst discrepancy between G3X2 and

TABLE 3: Phosphorus Oxides and Acids: Comparison of Computed Atomization Energies (kcal mol^{-1})

	atomization energy[a]							
	PO		PO_2		PO_3	HPO	HOPO	$HOPO_2$
method/reference state	UHF	ROHF[b]	UHF	ROHF[b]	UHF			
G3	143.54	143.05	264.15	263.06	360.79	211.92	362.60	480.76
UQCISD(T,full)/G3large[c]	143.69	142.36	265.00	263.11	361.69	211.87	362.37	480.84
G3X	146.72	143.66	265.79	264.13	363.39	213.23	364.64	483.51
G3X2	148.10	144.98	268.07	266.15	366.52	215.20	366.71	486.56
UQCISD(T,full)/G3Xlarge[d]	145.86	144.49	269.43	266.81	368.00	215.50	366.87	487.37
RCCSD(T)/TZ+CV[e]	135.16		253.10		346.14	204.35	352.11	466.70
RCCSD(T)/QZ+CV[e]	140.27		261.72		357.74	210.37	361.39	479.97
RCCSD(T)/5Z+CV[e]	142.12		264.83		361.89	212.39	364.43	N A
RCCSD(T)/CBS+CV[e]	144.05		268.09		366.25	214.51	367.61	489.65

[a] Not including zero-point energy. [b] All ROHF-based calculations performed at UB3LYP/6-31G(2df,p) geometries and use RCCSD(T) in place of QCISD(T) where appropriate. [c] Including G3 higher level correction. [d] Including G3X higher level correction. [e] Including core−valence correlation corrections, ref 42.

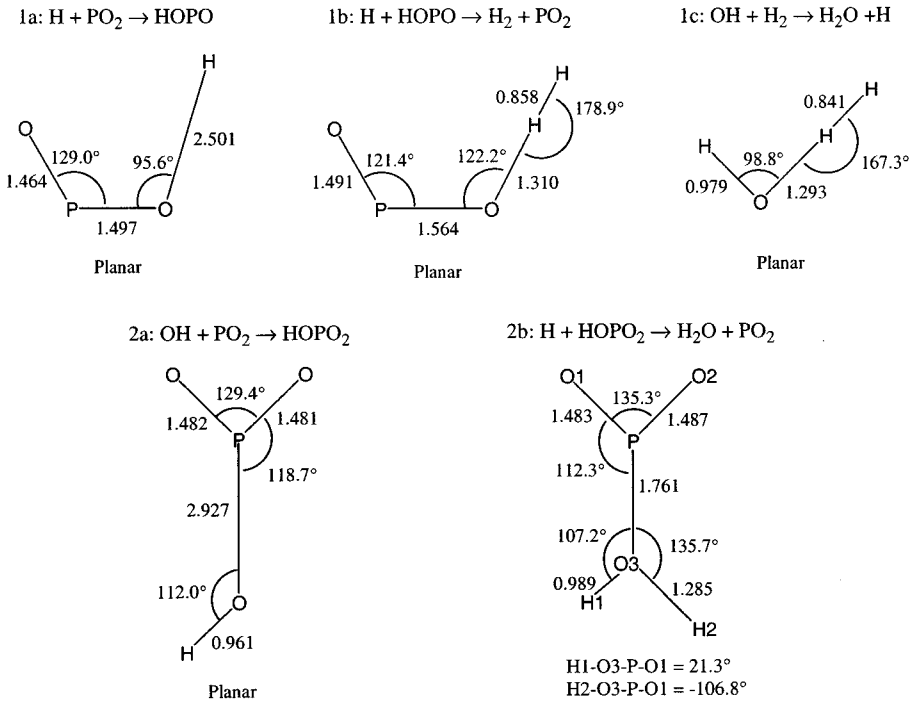

Figure 4. Geometries of transition states: Variational transition state geometries at 1000 K for reactions 1a and 2a obtained at CASSCF/cc-pVDZ level of theory. All others are saddle points computed at MP2/6-31G(d) level.

the CBS results occurs for $HOPO_2$, where the difference is 3.1 kcal mol^{-1}, although at the QCISD(T,full)/G3XLarge level it is reduced to 2.3 kcal mol^{-1}.

In light the encouraging performance of the G3X2 method for the above six molecules we have undertaken a larger systematic evaluation of G3X2, applying it to a larger number of phosphorus-containing molecules, including all those in Table 1. The results of this study will be published soon.

Kinetic Parameters. A primary aim of this work is the calculation of rate coefficients for the PO_2 + H and PO_2 + OH recombination reactions 1a and 2a, and for the subsequent abstraction reactions, viz., reactions 1b, 1c, and 2b. The rates of these reactions that make up the catalytic cycles are compared with the (experimental) rates of the (uncatalyzed) H + OH recombination reaction 3. The computed geometries of the transition states of these reactions are shown in Figure 4. The corresponding heats of formation at 298 K, rotational constants, and vibrational frequencies are summarized in Table 4. The geometries of the transition states of reactions 1b, 1c, and 2b correspond to well-defined first-order saddle points. However, the recombination reactions 1a and 2a are barrierless and thus require a VTST treatment to locate the geometries of the appropriate transition states at a given temperature, as outlined in the section on Theory and Computational Methods. The variational transition states were determined at five temperatures in the range 1000−2000 K. The parameters in Figure 4 and Table 4 pertaining to the transition states of reactions 1a and 2a were obtained at 1000 K. The full set of geometries, rotational constants, and vibrational frequencies are given in Tables S3 and S4 of the Supporting Information.

Given the barrierless nature of the recombination reactions 1a and 2a, initially we computed the dissociation rates of HOPO and $HOPO_2$ using RRKM, at a number of temperatures in the range 1000−2000 K, at pressures 1−10^4 Torr, for a bath gas of N_2. The heats of reactions involving phosphorus-containing species were computed using Bauschlicher's CBS heats of formation[42] (at 298 K) for PO_2, HOPO, and $HOPO_2$, and experimental literature values for all other species,[39−41,43] with the appropriate thermal corrections also taken from JANAF tabulations[39] or computed on the basis of the B3LYP geometries and frequencies.[42] The rate coefficients were then fitted to the Troe equations (8) − (13).[33] Figures 5−8 display the individual

TABLE 4: Computed Heats of Formation, Vibrational Frequencies, and Rotational Constants of Transition States[a]

reaction	$\Delta_f H_{298}^0$/kcal mol^{-1}	rotational constants/cm^{-1}	vibrational frequencies/cm^{-1}
1a: H + PO_2 → HOPO	−20.3	1.2566, 0.2936, 0.2380	340*i*, 82, 152, 406, 1022, 1329
1b: HOPO + H → PO_2 + H_2	−45.1	1.0019, 0.2722, 0.2140	2668*i*, 224, 270, 469, 774, 787, 899, 1276, 1477
1c: H_2 + OH → H_2O + H	12.9	18.5846, 2.9867, 2.5732	2813*i*, 628, 675, 1283, 1443, 3602
2a: PO_2 + OH → $HOPO_2$	−66.9	0.2919, 0.1124, 0.0812	200*i*, 86, 126, 164, 426, 470, 1087, 1212, 3982
2b: $HOPO_2$ + H → PO_2 + H_2O	−90.2	0.2708, 0.2481, 0.1321	3665*i*, 244, 279, 327, 438, 530, 632, 738, 1115, 1238, 1405, 3530

[a] Computed at 1000 K for variational transition states (1a, 2a).

TABLE 5: Computed Rate Coefficients: Troe,[a] Arrhenius,[b] and Modified Arrhenius[b] Fit Parameters

						high-pressure limit					low-pressure limit				
	Troe fit					Arrhenius		modified Arrhenius			Arrhenius		modified Arrhenius		
	a	1 − *a*	*T**	*T***	*T****	log *A*	E_a	log *A*	*n*	E_a	log *A*	E_a	log *A*	*n*	E_a
HOPO → PO_2 + H	1.00	0.00	950.72	4797.20	−115.31	15.34	94.9	13.57	0.50	93.6	16.57	82.1	34.97	−5.13	96.1
PO_2 + H → HOPO								10.06	1.29	−1.5			31.46	−4.33	1.02
HOPO + H → H_2 + PO_2[c]						14.28	16.1	7.33	1.94	10.8					
H_2 + OH → H_2O + H[c]						14.33	9.9	5.92	2.34	3.5					
$HOPO_2$ → HO + PO_2	1.00	-2.22×10^{-6}	640.64	3973.10	−202.75	15.56	105.2	24.44	−2.48	112.0	18.41	91.5	57.26	−10.83	121.0
HO + PO_2 → $HOPO_2$								14.19	−0.24	0.0			47.01	−8.59	9.0
$HOPO_2$ + H → PO_2 + H_2O[c]						14.10	26.7	8.74	1.49	22.6					

[a] See eqs 8− 13; *T**, *T***, *T**** in K. [b] See eqs 5 and 6; E_a in kcal mol^{-1}, *A* in s^{-1} or cm^3 mol^{-1} s^{-1}. [c] These reactions are not pressure dependent.

TABLE 6: Computed Enthalpies and Gibbs Free Energies of Reaction (in kcal mol^{-1}) at a Range of Temperatures

	H + PO_2 → HOPO		OH + PO_2 → $HOPO_2$	
T/K	$\Delta_r H_T^0$	$\Delta_r G_T^0$	$\Delta_r H_T^0$	$\Delta_r G_T^0$
298.15	−94.2	−86.6	−110.4	−99.1
1000	−95.4	−67.4	−110.0	−72.4
1250	−95.6	−60.4	−109.5	−63.1
1500	−95.7	−53.4	−108.9	−53.9
1750	−95.7	−46.3	−108.3	−44.7
2000	−95.7	−39.3	−107.6	−35.7

rate coefficients and the resulting Troe fits of these. Clearly, the quality of the fits is generally very good.

The calculated rate coefficients of all the reactions studied in this work, in the form of Troe, Arrhenius, or modified Arrhenius fits, are summarized in Table 5, in the temperature range 1000−2000 K. Further, pertinent computational details of the individual reactions are discussed below. The rate coefficients of the association, viz., recombination, were calculated by utilizing the appropriate equilibrium constants, as given by eq 7. Our calculated Gibbs free energies of reactions and reaction enthalpies at a number of temperatures are given in Table 6.

HOPO → H + PO_2. Initially, the potential energy surfaces of both the cis and trans isomers were studied in the region of dissociation at the CASSCF/cc-pVDZ level of theory. In the case of the trans isomer a saddle point was found at an O···H distance of 2.54 Å. This transition state was ∼ 7 kcal mol^{-1} higher in energy than the dissociation products H + PO_2. In contrast with such a 7 kcal mol^{-1} barrier to the recombination reaction to give the trans isomer, no barrier could be found for the dissociation of the lower energy cis isomer. This indicates that the latter mechanism represents the preferred reaction channel. The geometries and frequencies of the variational transition states were located at the CASSCF/cc-pVDZ level of theory. As the potential energy surface is very flat in the critical region, the transition state geometries at the various temperatures show little variation, as the data in Tables S3 and S4 of the Supporting Information indicate. The energies of the transition states relative to the dissociated products were obtained from CASSCF/cc-pVDZ calculations.

H + HOPO → H_2 + PO_2 and **OH + H_2 → H_2O + H.** The transition state geometries (corresponding to first-order saddle points) and critical energies were computed at the G3 level of theory.

$HOPO_2$ → OH + PO_2. The geometries of the variational transition states were located at the CASSCF/cc-pVDZ level of theory. The energies of the transition states relative to the dissociated products were calculated at the CASPT2/cc-pVTZ level. As before, the enthalpy of dissociation was determined using Bauschlicher's[42] CBS heats of formation (at 298 K) for PO_2 and $HOPO_2$ and experimental values for OH.

H + $HOPO_2$ → H_2O + PO_2. The search for a transition state for this reaction initially yielded a minimum corresponding to a weakly bound PO_2···H_2O dimer. This dimer had a binding energy of 4.8 kcal mol^{-1} after applying the counterpoise correction for basis set superposition effects. However, from the point of view of this work the existence of such a dimer is of academic interest only, as it would not be expected to be stable at ∼ 2000 K. The transition state for OH abstraction by H is characterized by a long OH bond and a slightly elongated PO bond. The geometry and barrier height were located at the G3 level of theory.

Finally, our calculated rate coefficients at the temperatures of 1000 and 2000 K and a pressure of 532 Torr are summarized in Table 7 where they are compared with Twarowski's estimated values (which were obtained by the application of Benson's rules), the modeling values of Korobeinichev et al.[13] and experiment.[45]

At 2000 K the rate coefficients in the two reaction schemes considered are comparable in magnitude, suggesting that both routes are important, in qualitative agreement with Twarowski's conclusions. However, in an absolute sense, the rate coefficients obtained in this work are significantly lower than Twarowski's, especially at 1000 K, although order of magnitude differences can exist even at the higher temperature. Our values agree somewhat better with the modeled values of Korobeinichev et

TABLE 7: Comparison of Computed and Experimental Rate Coefficients at 532 Torr Pressure at 1000 and 2000 K (in cm^3 mol^{-1} s^{-1})

reaction	T (K)	k (this work)	k (Twarowski[a])	k (Korobeinichev et al.[b])	k (expt)
1a: $PO_2 + H \rightarrow HOPO$	1000	7.03×10^{12}	4.42×10^{12} [c]	4.55×10^{13} [c]	
	2000	2.78×10^{11}	2.87×10^{11} [c]	6.51×10^{12} [c]	
1b: $HOPO + H \rightarrow H_2 + PO_2$	1000	6.08×10^{10}	3.15×10^{13}	7.70×10^{11}	
	2000	3.53×10^{12}	3.16×10^{13}	7.80×10^{11}	
1c: $H_2 + OH \rightarrow H_2O + H$	1000	1.52×10^{12}	6.28×10^{13}		1.26×10^{12} [d]
	2000	1.88×10^{13}	6.30×10^{13}		8.33×10^{12} [d]
2a: $HO + PO_2 \rightarrow HOPO_2$	1000	7.40×10^{12}	1.74×10^{14} [c]	1.71×10^{13} [c]	
	2000	3.68×10^{11}	5.62×10^{12} [c]	1.89×10^{12} [c]	
2b: $HOPO_2 + H \rightarrow PO_2 + H_2O$	1000	1.93×10^{8}	3.16×10^{13}	1.55×10^{9}	
	2000	1.60×10^{11}	3.16×10^{13}	3.13×10^{10}	
3: $H + OH \rightarrow H_2O$	1000		3.56×10^{9} [c]		7.12×10^{12} [c,e]
	2000		1.17×10^{9} [c]		8.91×10^{9} [c,e]

[a] Ref 3. [b] Ref 13. [c] Calculated as k[M]. [d] Fit to all NIST data, ref 46. [e] Ref 45.

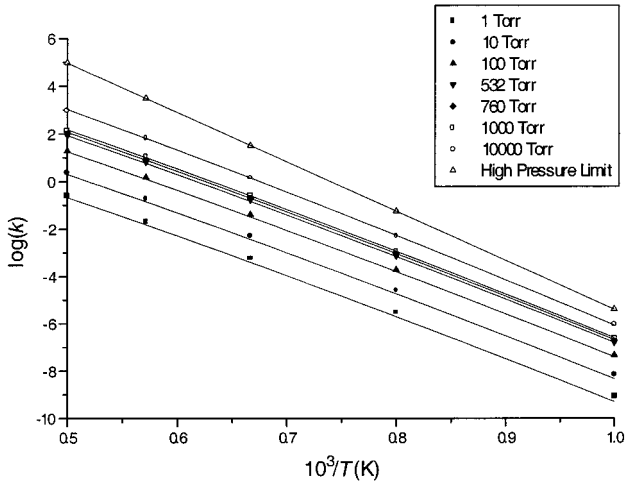

Figure 5. Arrhenius plots of RRKM rate constants for HOPO → PO_2 + H reaction at a range of pressures. (Symbols = computed rate constants; Lines = Troe fits.)

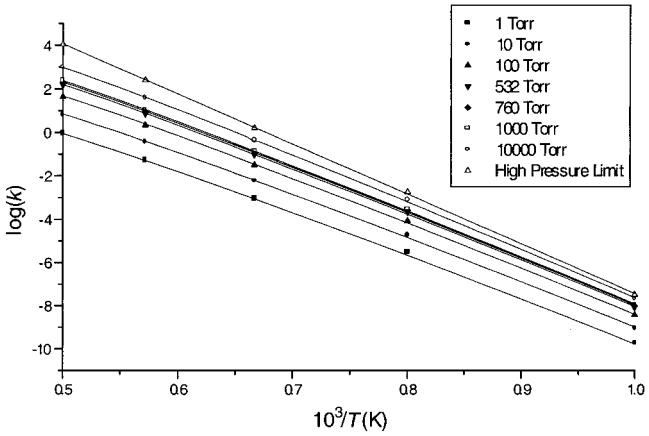

Figure 6. Arrhenius plots of RRKM rate constants for $HOPO_2$ → PO_2 + OH reaction at a range of pressures. (Symbols = computed rate constants; Lines = Troe fits.).

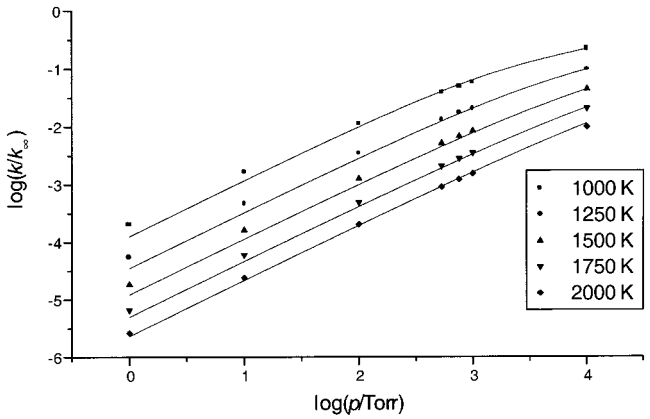

Figure 7. Pressure dependence of RRKM rate constants for HOPO → PO_2 + H reaction at a range of temperatures. (Symbols = computed rate constants; Lines = Troe fits.).

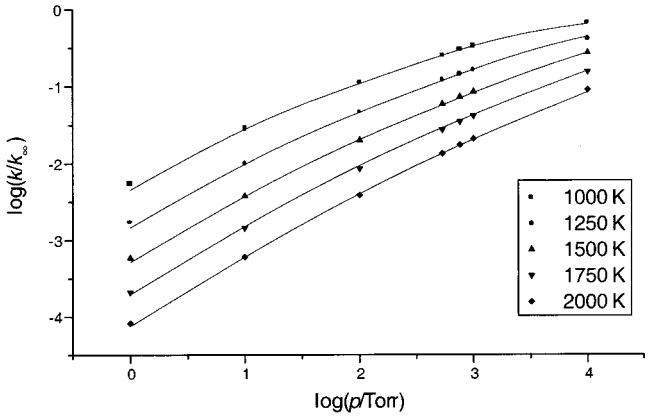

Figure 8. Pressure dependence of RRKM rate constants for $HOPO_2$ → PO_2 + OH reaction at a range of temperatures. (Symbols = computed rate constants; Lines = Troe fits.).

al.,[13] but there remain significant differences. Under the conditions studied by Twarowski (0.7 atm pressure and 1970 K) the rate coefficient for reaction 1a is substantially into the falloff region (approximately 1000-fold lower than the high pressure limit), whereas the coefficient for reaction 2a is significantly less so (only ~60-fold lower than the high-pressure limit). Thus while it might be acceptable to use the termolecular rate coefficient for reaction 1a in modeling, in light of its proximity to the limiting low-pressure value, the appropriate falloff value of the rate coefficient should be used for reation 2a. For the H_2 + OH abstraction reaction 1c the computed G3 rate coefficients agree with the observed values[46] to within a factor of approximately two or better, depending on the temperature.

Conclusion

Using ab initio quantum chemical and RRKM techniques theoretical rate coefficients were obtained for the H + PO_2 (reaction 1a) and OH + PO_2 (reaction 2a) recombination reactions and for the subsequent H + HOPO (reaction 1b) and H + $HOPO_2$ (reaction 2b) abstraction reactions, which, along with the OH + H_2 abstraction reaction 1c constitute the catalytic pathway for the H + OH recombination reaction 3, as formulated by Twarowski [1−4] and also by Korobeinichev et al.[13]

Our computed rate coefficients for reaction 1c agree well with experiment (within 20% at 1000 K and almost within a factor of 2 at 2000 K), while for the other reactions our rate coefficients are consistent with the modeled values of Korobeinichev et al.,[13] although for several key reactions (1b, 2a, 2b) they are substantially lower than Twarowski's values. While we utilized Bauschlicher's[42] recent thermochemical data in the derivation of our rate coefficients, we note that reasonable accuracy could be achieved by the application of the G3X and G3X2 methods to the computation of the heats of formation of the phosphorus-containing species. Using the G2, G3, and G3X methods we also computed the thermochemistry of Twarowski's reaction model which includes 17 phosphorus-containing molecules.

Acknowledgment. N.L.H. gratefully acknowledges the award of an Australian Postgraduate Research Scholarship.

Supporting Information Available: Tables S1−S4 containing geometries, rotational constants, and vibrational frequencies. This material is available free of charge via the Internet at http://pubs.acs.org.

References and Notes

(1) Twarowski, A. *Combust. Flame* **1993**, *94*, 91.
(2) Twarowski, A. *Combust. Flame* **1993**, *94*, 341.
(3) Twarowski, A. *Combust. Flame* **1995**, *102*, 41.
(4) Twarowski, A. *Combust. Flame* **1996**, *105*, 407.
(5) Benson, S. W. *Thermochemical Kinetics*; John Wiley: New York, 1976.
(6) Curtiss, L. A.; Raghavachari, K.; Trucks, G. W.; Pople, J. A. *J. Chem. Phys*. **1991**, *94*, 7221.
(7) Curtiss, L. A.; Raghavachari, K.; Redfern, P. C.; Rassolov, V.; Pople, J. A. *J. Chem. Phys*. **1998**, *109*, 7764.
(8) Curtiss, L. A.; Redfern, P. C.; Raghavachari, K.; Pople, J. A. *J. Chem. Phys*. **2001**, *114*, 108.
(9) Macdonald, M. A.; Jayaweera, T. M.; Fisher, E. M.; and Gouldrin, F. C. *Combust. Flame* **1999**, *116*, 166.
(10) Green, J. *J. Fire Sci.* **1996**, *14*, 426.
(11) Dempsey, C. R.; Oppelt, E. F. *Air Waste* **1993**, *43*, 25.
(12) Korobeinichev, O. P.; Ilyin, S. B.; Bolshova, T. A.; Shvartsberg, V. M.; Chernov, A. A. *Combust. Flame* **2000**, *121*, 593.
(13) Korobeinichev, O. P.; Ilyin, S. B.; Bolshova, T. A.; Shvartsberg, V. M.; Chernov, A. A. *Combust. Flame* **2001**, *125*, 744.
(14) Macdonald, M. A.; Gouldin, F. C.; Fisher, E. M. *Combust. Flame* **2001**, *125*, 668.
(15) Curtiss, L. A.; Raghavachari, K.; Redfern, P. C.; Pople, J. A. *J. Chem. Phys*. **1997**, *106*, 1063.
(16) Henry, D. J.; Radom, L. In *Theoretical Thermochemistry*; Cioslowski, J., Ed.; Kluwer: Dordrecht, 2001.
(17) Mayer, P. M.; Parkinson, C. J.; Smith, D. M.; Radom, L. *J. Chem. Phys*. **1998**, *108*, 604.
(18) Parkinson, C. J.; Mayer, P. M.; Radom, L. *J. Chem. Soc., Perkin Trans. 2* **1999**, *11*, 2305.
(19) Pople, J. A.; Head-Gordon, M. A.; Raghavachari, K. *J. Chem. Phys*. **1987**, *87*, 5968.
(20) Raghavachari, K.; Trucks, G. W.; Pople, J. A.; Head-Gordon, M. *Chem. Phys. Lett*. **1989,** *157*, 479.
(21) Hampel, C.; Peterson, K.; Werner, H.-J. *Chem. Phys. Lett*. **1992**, *190*, 1.
(22) Steinfeld, J. I.; Francisco, J. S.; Hase, W. L. *Chemical Kinetics and Dynamics*; Prentice Hall: Englewood Cliffs, NJ, 1989; p 308.
(23) McQuarrie, D. A. *Statistical Mechanics*; Harper & Row: New York, 1973; p 129.
(24) (a) Pollack, E. In *Theory of Chemical Reaction Dynamics*; Baer, M., Ed; CRC Press: Boca Raton, 1985; Vol. 3, p 128. (b) Truhlar, D. G.; Garrett, B. C. *Acc. Chem. Res*. **1980**, *13*, 440. (c) Hase, W. L.; Mondro, S. L.; Duchovic, R. J.; Hirst, D. M. *J. Am. Chem. Soc*. **1987**, *109*, 2016.
(25) Bacskay, G. B.; Martoprawiro, M.; Mackie, J. C. *Chem. Phys. Lett*. **1999**, *300*, 321.
(26) Sendt, K.; Bacskay, G. B.; Mackie, J. C. *J. Phys. Chem. A* **2000**, *104*, 1861.
(27) Roos, B. O.; Taylor, P. R.; Siegbahn, P. E. S. *Chem. Phys*. **1980,** *48*, 157.
(28) Roos, B. O. In *Ab Initio Methods in Quantum Chemistry*; Lawley, K. P., Ed.; Wiley: Chichester, U.K. 1987; Vol. 2, p 399.
(29) Dunning, T. H. *J. Chem. Phys*. **1987**, *90*, 1007.
(30) Woon, D. E.; Dunning, T. H. *J. Chem. Phys*. **1990**, *98*, 1358.
(31) Andersson, K.; Malmqvist, P.-Å.; Roos, B. O.; Sadlej, A. J.; Wolinski, K. *J. Chem. Phys*. **1990**, *94*, 5483.
(32) Andersson, K.; Malmqvist, P.-Å.; Roos, B. O. *J. Chem. Phys*. **1992,** *96*, 1282.
(33) Gilbert, R. G.; Luther, K.; Troe, J. *Ber. Bunsen-Ges. Phys. Chem*. **1983**, *87*, 169.
(34) Frisch, M. J.; Trucks, G. W.; Schlegel, H. B.; Scuseria, G. E.; Robb, M. A.; Cheeseman, J. R.; Zakrzewski, V. G.; Montgomery, J. A.; Stratmann, R. E.; Burant, J. C.; Dapprich, S.; Millam, J. M.; Daniels, A. D.; Kudin, K. N.; Strain, M. C.; Farkas, O.; Tomasi, J.; Barone, V.; Cossi, M.; Cammi, R.; Mennucci, B.; Pomelli, C.; Adamo, C.; Clifford, S.; Ochterski, J.; Petersson, G. A.; Ayala, P. Y.; Cui, Q.; Morokuma, K.; Malik, D. K.; Rabuk, A. D.; Raghavachari, K.; Foresman, J. B.; Cioslowski, J.; Ortiz, J. V.; Stefanov, B. B.; Lui, G.; Liashenko, A.; Piskorz, P.; Komaromi, I.; Gomperts, R.; Martin, R. L.; Fox, D. J.; Keith, T.; Al-Laham, M. A.; Peng, C. Y.; Nanayakkara, A.; Gonzalez, C.; Challacombe, M.; Gill, P. M. W.; Johnson, B. G.; Chen, W.; Wong, M. W.; Andres, J. L.; Head-Gordon, M.; Replogle E. S.; Pople, J. A. *Gaussian 98* (Revision A.7); Gaussian, Inc., Pittsburgh, PA, 1998.
(35) ACES II is a program product of the Quantum Theory Project, University of Florida. Authors: Stanton, J. F.; Gauss, J.; Watts, J. D.; Nooijen, M.; Oliphant, N.; Perera, S. A.; Szalay, P. G.; Lauderdale, W. J.; Gwaltney, S. R.; Beck, S.; Balková, A.; Bernholdt, D. E.; Baeck, K.-K.; Rozyczko, P.; Sekino, H.; Hober, C.; Bartlett, R. J. Integral packages included are VMOL (Almlöf, J.; Taylor, P. R.); VPROPS (Taylor, P.); ABACUS (Helgekar, T.; Jensen, H. J. Aa.; Jørgensen, P.; Olsen, J.; Taylor, P. R.)
(36) "DALTON, an ab initio electronic structure program, Release 1.0 1997" written by Helgaker, T.; Jensen, H. J. Aa.; Joergensen, P.; Olsen, J.; Ruud, K.; Aagren, H.; Andersen, T.; Bak, K. L.; Bakken, V.; Christiansen, O.; Dahle, P.; Dalskov, E. K.; Enevoldsen, T.; Fernandez, B.; Heiberg, H.; Hettema, H.; Jonsson, D.; Kirpekar, S.; Kobayashi, R.; Koch, H.; Mikkelsen, K. V.; Norman, P.; Packer, M. J.; Saue, T.; Taylor, P. R.; Vahtras, O.
(37) Andersson, K.; Blomberg, M. R. A.; Fülscher, M. P.; Karlström, G.; Lindh, R.; Malmqvist, P.-Å.; Neogrády, P.; Olsen, J.; Roos, B. O.; Sadlej, A. J.; Schültz, M.; Seijo, L.; Serrano-Andrés, L.; Siegbahn, P. E. M.; Widmark, P.-O. MOLCAS Version 4; Lund University: Lund, Sweden, 1997.
(38) Mokrushin, V.; Bedanov, V.; Tsang, W.; Zachariah, M.; Knyazev, V. ChemRate Version 1.10; National Institue of Standards and Technology: Gaithersburg, MD, 1999.
(39) Chase, M. W., Jr. *NIST-JANAF Thermochemical Tables*, 4th ed.; *J. Phys. Chem. Ref. Data* **1998**, *Monograph 9*, 1.
(40) Rusic, B.; Feller, D.; Dixon, D.; Peterson, K. A.; Harding, L. B.; Asher, R. L.; Wagner, A. F. *J. Phys. Chem. A* **2001**, *105*, 1.
(41) Drowart, J.; Myers, C. E.; Szwarc, R.; Vander Auwera-Mahieu, A.; Uy, O. M. *J. Chem. Soc., Faraday Trans. 2* **1972**, *68*, 1749.
(42) Bauschlicher, C. W., Jr. *J. Phys. Chem*. **1999**, *103*, 11126.
(43) Hildenbrand, D. L.; Lau, K. H. *J. Chem. Phys*. **1994**, *100*, 8373.
(44) Curtiss, L. A.; Raghavachari, K.; Redfern, P. C.; Pople, J. A. *J. Chem. Phys*. **2000**, *112*, 7374.
(45) Baulch, D. L.; Cobos, C. J.; Cox, R. A.; Esser, C.; Frank, P.; Just, Th.; Kerr, J. A.; Pilling, M. J.; Troe, J.; Walker, R. W.; Warnatz, J. *J. Phys. Chem. Ref. Data* **1992**, *21*, 411.
(46) Mallard, W. G.; Westley, F.; Herron, J. T.; Hampson, R. G.; Frizzell, D. H. NIST Chemical Kinetic Database: Version 2Q98, Dec. 1998, National Institute of Standards and Technology: Gaithersburg, MD 20899.